Uppsala University
Department of Physics and Astronomy

UPPSALA
UNIVERSITET

Superluminous magnons in Nickel Oxide

Master's Thesis

Jannes van Poppelen

Supervisors:
Oscar Grånäs
Anders Bergman

Subject reader: Jonas Fransson
Examiner: Andreas Korn

Abstract

Recent experiments have shown that the magnon velocity over nanoscale distances in certain antiferromagnetic materials, with NiO in particular, far exceeds the previous theoretical maximum. Antiferromagnetic insulators are excellent candidates for spintronic nanodevices due to their exceptionally low energy dissipation, which could benefit the future speed at which information is stored. These magnons, which have since been dubbed "superluminous-like magnons", are classically not expected, and it is hypothesized that the presence of a damping term in the equation of motion of the magnetic moment accounts for this anomalous behaviour.
In this work, spin dynamics simulations are done using the UppASD software package in order to verify the existence of these superluminous-like magnons, where the magnon velocity in NiO is determined through a variety of ways. Analyzing simulated magnon spectra around high-symmetry points where the dispersion is linear allows for an extraction of magnon velocities, which shows no abnormal behaviour for bulk NiO, as well as for large wavelength (low energy) magnons. Other ways to determine the magnon velocity have been performed by studying the propagation of magnons that are excited through various methods. These studies also show that the magnon velocity does not far exceed the previous theoretical limit. While these magnons propagate slightly faster than they would in bulk, it is shown that these magnons very rapidly decelerate to their known bulk speeds.

Populärvetenskaplig sammanfattning

I de flesta elektroniska apparater idag lagras information i så kallade magnetiska bitar, som antar ett av två möjliga värden: 1 eller 0. Genom att kontrollera bitarnas värde kan information avläsas och lagras. Informationshanteringen genomförs av kvasipartiklar, så kallade magnoner, som skapas genom att applicera externa magnetfält till lagringsmediet. Magnoner beter sig som partiklar, trots att de inte formellt betraktas som sådana - därav klassificeras de som kvasipartiklar. Ju högre magnonhastigheten är, desto snabbare är informationslagringen. Därför eftersträvas så höga hastigheter som möjligt.

I nyligen utförda experiment har det påvisats att magnonhastigheten över väldigt korta avstånd i vissa magnetiska material kan överskrida de teoretiska förutsägelserna avsevärt. Dessa specifika magnoner, vars hastighet är markant högre än man tidigare förutsätt, kallas "överljusfarts aktiga partiklar". Det anmärkningsvärda med dessa partiklar är att rörelseekvationerna som beskriver magnoners rörelse i magnetiska material inte förutspår en möjlig överljushastighet. En hypotes som har presenterats för att förklara fenomenet, är att en dämpning i rörelseekvationerna utgör källan för magnoner som rör sig med överljushastighet. Denna förklaring kan dock tyckas vara kontraintuitiv eftersom en dämpande faktor innebär ett minskande av energi från magnonerna, vilket borde leda till lägre hastigheter.

För att verifiera existensen av magnoner med överljusfart, simuleras magnetiska system på atomnivå genom att använda mjukvarupaketet UppASD. Magnonhastigheten för ett stort antal olika dämpningsfaktorer beräknas med olika metoder. Eftersom det finns ett direkt samband mellan magnonens energi och dess hastighet, bestäms energispektrumet för magnoner med låg energi, Spektrumet beskriver magnonernas energi på flera ställen i de enskilda kristallerna, som tillsammans utgör bulken för det magnetiska materialet. De andra metoderna skapar magnoner genom att införa lokala störningar i den magnetiska ordningen, antingen manuellt eller genom att indirekt lägga på korta laserpulser vilka sedan följs då de fortskrider genom materialet. Genom att undersöka hur länge det tar för varje magnon att nå specifika atomer i materialet kan en bra uppskattning göras för hur snabbt magnonerna har färdats.

Intressant nog verkar det som att magnonhastigheten i alla olika undersökta fall inte är i närheten av att nå extremt höga värden. Dessutom verkar dämpningkoefficienterna - som borde vara orsaken till överljushastigheten - ha en minimal inverkan på magnonhastigheten. Denna observation stämmer väl överens med såväl klassiska - som den kvantmekaniska teorin. Det visar sig att ett möjligt misstag kan ha gjorts under utförandet av de fysiska experimenten. Således är det enda sättet att verifiera existensen för magnoner som rör sig med överljusfart att reproducera dem genom att utföra samma experiment igen, men den här gången med större noggrannhet in i minsta detalj.

Contents

1 Introduction

Spintronics is a rapidly developing technology that exploits the spin of the electron and the associated magnetic moment thereof. Its most prominent use nowadays is in the field of high-speed data storage and reading of hard drives. The magnetic storage of information on various media is governed by single-domain magnetic nanoparticles [1]. The storage medium can be divided into various sections, also known as bits. Due to the quantized nature of the magnetic moment, there are only two types of bits. For bits in which a magnetic field is measured, a '1' is detected, whereas, for bits in the absence of a magnetic field, a '0' is detected. In order to store information, one needs to be able to manipulate the value of these bits. This is achieved through a variety of magnetic excitations. One such excitation is a spin wave. When a magnetic system gets excited, its ordered magnetic moments start precessing. On a slightly bigger scale, it looks as if neighbouring magnetic moments propagate as a wave through the lattice, due to the presence of a constant phase difference between neighbours. Similar to how phonons are the quanta for lattice excitations, spin waves are also quantized, and have their own quanta; the magnon. A different description of magnetism depending on the itinerant nature of the valence electrons gives rise to a different kind of magnetic excitation. Stoner excitations arise between electrons and holes in different bands [2]. When an electron gets excited in a system having more electrons than holes, the electron will leave behind a hole in the valence band, which essentially means that the sign of the magnetic moment gets flipped. Stoner excitations are hence also known as spin-flip excitations. This excitation is of crucial importance in allowing the changing of bits in the storage medium. Spin waves and Stoner excitations are also related. Finite energy spin waves decay into Stoner excitations, which then account for the finite lifetimes of the spin waves.

As the amount of data that needs to be stored is continuously increasing, faster methods to store this data are of crucial importance. One promising approach is the use of antiferromagnetic (AFM) materials in spintronics over the more conventional ferromagnetic (FM) materials. AFMs have a fundamentally different lattice structure compared to regular FMs. While their chemical structure can be similar, their magnetic ordering is vastly different as the magnetic moments for AFMs align in a regular pattern directed opposite to their neighbouring magnetic moments.

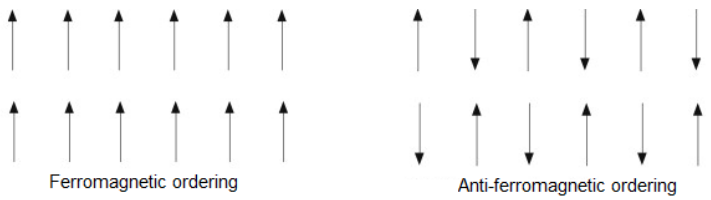

Figure 1: Illustration of the magnetic ordering of both ferromagnetic and antiferromagnetic materials.

As a result, AFMs have no net magnetization and as a consequence will be insensitive to external magnetic fields. Recent discoveries have shown that AFMs can

be controlled electrically, similar to FMs, making them promising candidates for all kinds of spintronic nano-devices, as they are far more common in nature than their FM counterparts [3]. AFM materials have several other benefits in the field of spintronics over using FM materials as their magnetic dissipation is low, which is of considerable interest when aiming to construct energy-efficient devices.

1.1 Superluminal-like magnons in NiO

Recent experiments have shown that certain AFM materials, with nickel oxide (NiO) in particular, can excite magnons that could potentially reach "superluminal-like" speeds at nanoscale distances [4]. For this experiment one typically starts with a non-magnet (NM)/FM bilayer, as seen in figure 2 below. Optical excitation of the FM induces a spin current that propagates through the NM. Analogous to how electric currents have their purpose in electronics, spin currents serve as a way to carry information in spintronics. Upon reaching the NM this spin current is then converted into a charge current via spin-charge-conversion through for example the inverse spin Hall effect [5]. This charge current is time-dependent due to the short-pulsed optical excitation of the FM and hence it emits radiation, typically with frequencies in the range of terahertz (THz) [6]. These signals can be observed and studied using THz spectroscopy.
A similar setup is used to study the magnonic properties of AFM materials. This time the AFM is insulated between the FM/NM bilayer, forming a trilayer. Typical widths of this AFM layer are in the range of several dozens of nanometers. Once again the FM layer will be optically excited, but now the spin current generated in the FM will induce a magnon current in the AFM. The magnon current transfers some angular momentum to the NM, which then generates the measurable THz signal like before.
The introduction of the AFM layer introduces a time delay when measuring the THz signal due to the time it takes the magnon to propagate through the AFM. Measuring this time delay, and using the width on the insulated AFM makes it possible to determine the magnon velocity in the AFM, simply by dividing the width of the AFM layer by the measured time delay. High magnon velocities are critical in the construction of these nanodevices as it allows for higher operating speeds. This results in lower operation times and hence also less power consumption by these devices. Measured magnon velocities in several materials have shown to far exceed theoretical estimates, giving rise to the name "superluminous-like magnons". Interestingly enough it turns out that the measured magnon velocity also has a non-trivial dependence on the thickness of the AFM, which requires some further investigation.

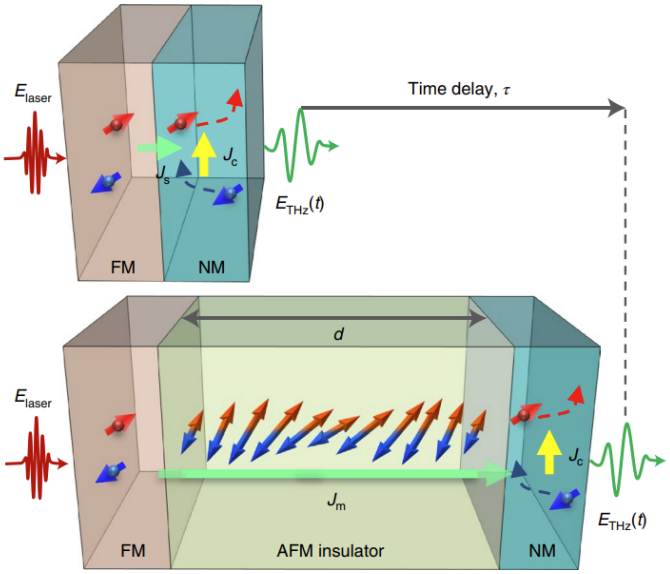

Figure 2: Experimental set-ups for the measurement of superluminal-like magnons. The upper setup is the FM/NM bilayer, whereas the lower setup also contains the insulated AFM. Figure taken from [4].

Repeated measurements of the magnon velocities with varying thicknesses of the AFM layer suggest that the maximum magnon velocity is related to the improved AFM ordering in the AFM, as the thickness increases. It has been hypothesized that a dampening term in the equations of motion governing the spin dynamics can account for these superluminous magnons as it would make dispersion anomalous for large wavelength magnons. While it may sound counter-intuitive for a dampening effect to have a beneficial contribution to magnon velocities, it is not a novelty as superluminal-like group velocities have been previously known to exist for various dissipative materials in the fields of optics and electronics [7]. This phenomenon is of considerable interest as it allows for pushing the fundamental limit of these spintronic nanodevices.

1.2 Thesis outline

Classically, these superluminal-like magnon velocities are not expected. As such, the original paper on these superluminous magnons is of considerable interest and deserves a closer look. This thesis will investigate these superluminal-like magnon velocities, as well as try to reproduce these magnon velocities, if not produce classically expected ones, through spin dynamics simulations. Chapter two of this thesis presents the necessary parts of the theories of magnetism and spin dynamics and relates them with magnon velocities. In chapter three, UppASD and the various methods to compute magnon velocities through spin dynamics simulations are elaborated. Chapters four and five present and discuss the obtained results, respectively. Additionally, comparisons between magnon velocities with the original paper [4] are made.

2 Magnetism and NiO

Magnetism in its most fundamental form is the study of magnetic moments in materials. Solids get their magnetic properties from the magnetic moments of valence electrons so that our current understanding of magnetism has its roots in quantum mechanics, without which static magnetism would not even exist in the first place. The two kinds of quantized angular momenta of electrons, the spin part, and the orbital momentum part, together make up for its total angular momentum. These two are further linked together by the relativistic spin-orbit coupling (SOC). When coupled to the gyromagnetic ratio, γ, the total angular momentum also makes up the total magnetic moment of electrons. While nuclear spins also give rise to magnetic moments, they are much smaller in size than the electronic spin due to the significantly higher nucleon mass and are hence often negligible. Aside from the relativistic corrections to the energy spectrum of hydrogen, SOC also gives rise to a handful of magnetic interactions and nanostructures, such as magnetic anisotropies and skyrmions. The former, together with a handful of other magnetic interactions, will be of particular interest to this study.
This section will build the framework for studying magnon velocities within NiO. First, the various relevant kinds of magnetic interactions will be elaborated on. Then the crystal structure of NiO will be explored some more. This will be followed up by deriving the classical dispersion relation and group velocity for magnons in NiO, using the so-called Landau-Lifshitz-Gilbert (LLG) equation of motion for the magnetic moments. Finally, spin correlation functions of magnetic moments are connected to the magnon dispersion relation.

2.1 Magnetic interactions

The Hamiltonian of magnetic systems consists of a variety of magnetic interactions, which, coupled with the LLG equation, completely, in a classical sense, describe the dynamics of magnetic moments within them. Some of these interactions are quite exotic and can for instance arise when systems lack certain symmetries, such as the Dzyaloshinskii-Moriya interaction [8, 9]. NiO, however, is highly symmetric and will not be subject to this interaction. Other interactions are the result of relativity, like magnetocrystalline anisotropy (MCA). Often, the most dominant magnetic interaction is quantum mechanical in nature. This exchange interaction only affects indistinguishable particles, such as electrons. All in all, the relevant interactions are contained in the magnetic Hamiltonian, which is given by

$$\mathcal{H} = \mathcal{H}_{EX} + \mathcal{H}_Z + \mathcal{H}_{MCA} + \mathcal{H}_D, \tag{1}$$

where $\mathcal{H}_{EX}$ is the exchange interaction, $\mathcal{H}_{MCA}$ is the contribution due to MCAs, $\mathcal{H}_D$ is the regular dipole energy and $\mathcal{H}_Z$ is the classical Zeeman term, all of which will be clarified in their respective sections below.

2.1.1 Exchange interaction

The Pauli exclusion principle forbids two electrons from occupying the same state. Instead, each electron will occupy a state with a different spin configuration, either of them slightly different in their respective energies. The repulsion due to the

Coulomb interaction, together with these split states, is the origin of the exchange interaction.
To further clarify this, it is useful to consider a system consisting of two electrons, such as the helium atom. Again the Pauli exclusion principle requires the total wave function of this system, denoted by Ψ, to be completely antisymmetrical under the exchange of the two electrons. If the Hamiltonian of the system does not explicitly contain a term involving spin, then Ψ is made up of two separate parts

$$\Psi = \psi \otimes \chi, \tag{2}$$

in which ψ is a spatial contribution, and χ is a spin contribution. Antisymmetrization of Ψ forces it to take one of two forms

$$\Psi_1 = \psi_s \otimes \chi_a \text{ or } \Psi_2 = \psi_a \otimes \chi_s, \tag{3}$$

where the subscripts s and a mean are symmetric and antisymmetric under the exchange of two electrons, respectively. For spin-$\frac{1}{2}$ particles, such as the electron, these symmetric and antisymmetric take the form of the usual triplet and single states, due to how the spin representation of the composite system decomposes [10].
Magnetism affects many electrons at the same time. This requires some electrons to occupy excited states. The energy necessary to push these electrons to this state is provided by the repelling Coulomb interaction. The two different antisymmetric wave functions have different energies associated with them depending on the parity of the spatial projection. The energy of the states can simply be computed as the ground state energy through the expectation value of the Hamiltonian, whose potential part is given by the Coulomb interaction. Explicit evaluation of these energies in one's favourite basis yields that the Coulomb interaction prefers antisymmetric spin configurations of the wave function, as these tend to have lower energies. The contribution of the spatial projection of the wavefunction to the energy in a basis of position eigenstates takes the form of

$$\mathcal{E} = \int \psi^*_{s,a}(r_1, r_2)\mathcal{H}\psi_{s,a}(r_1, r_2)dr_1^3 dr_2^3, \tag{4}$$

where the integrals are taken over the configuration space of both electrons. One can define a corresponding exchange parameter J as half of the energy difference between the energies of the antisymmetric- and symmetric spin configurations so that the exchange energy is given by

$$\Delta E = -2J\mathbf{m}_1 \cdot \mathbf{m}_2, \tag{5}$$

where $\mathbf{m}_{1,2}$ is the dimensionless spin configuration of the first and second electron, respectively, which ensures that the exchange parameter takes on the units of energy. The inner product that arises here is a result of the norm in the spin space.
This energy was later generalized by Heisenberg to many-electron systems, giving rise to the classical Heisenberg Hamiltonian, which for a lattice with atoms on sites i and j reads,

$$\mathcal{H} = -\sum_{\substack{i,j \\ i \neq j}} J_{ij}\mathbf{m}_i \cdot \mathbf{m}_j, \tag{6}$$

where J_{ij} is the exchange parameter between atoms on sites i and j. From henceforth, for brevity, whenever magnetic moments are mentioned, these always mean magnetic moments specified at sites on a lattice. Note that the factor in front- and the sign of exchange parameter is ambiguous and there exists no clear consensus on which to use, so this explicit form of the Hamiltonian, in which the factor of 2 is absorbed within the J, will be used throughout this work. This exchange mechanism is also responsible for spontaneous magnetization. The sign of the exchange parameters is of crucial importance in a material's magnetic ordering. Materials that have $J_{ij} > 0$ are said to behave ferromagnetically, whereas materials that have $J_{ij} < 0$ behave antiferromagnetically. It is seemingly impossible to directly experimentally determine the values of the exchange parameters, meaning that one typically has to resort to studying experimentally determined magnon spectra. Alternatively, the values of the exchange parameters can be computed more rigorously via a first-principle approach using local spin density functionals, where the linear response of the ground state energy subject to small excitations of on-site magnetic moments has been thoroughly analyzed and computed [11–13].

While there exists no classical analogue to the exchange interaction, this Hamiltonian is still seen as classical, but this is due to the fact that it can be quantized even further, where the spin operators are transformed into creation and annihilation operators [14]. The Heisenberg Hamiltonian generalizes the well-known Ising model, whose original purpose was to act as the simplest description of FM, as well as the identification of phase transitions.

Even though the Coulomb interaction is a fairly long-ranged interaction, the resulting exchange interaction is short-ranged, with nearest neighbour- (NN) and next-nearest neighbour (NNN) couplings bringing in the predominant contributions. The exchange interaction in NiO works just a bit differently than it would in body-centered cubic iron (bcc Fe). The d-electrons in insulators and transition metals such as NiO are localized, and hence there is not a lot of overlap between the 3d-orbitals of nickel atoms. Nickel atoms are too far separated in order to allow a strong direct exchange interaction, meaning that NN exchange parameters in NiO are practically negligible if not zero. In bcc Fe, the iron atoms are sufficiently close to each other to allow a direct exchange interaction. However, nickel 3d-orbitals hybridize with oxygen 2p-orbitals, as seen in figure 3 below, forming, what looks like an "oxygen bridge", between NNN nickel atoms. This oxygen bridge then admits what is known as a superexchange interaction, allowing electrons to move freely between NNN nickel atoms, using the oxygen atoms which results in a stronger exchange coupling [15]. This mechanism is further made possible because the oxygen ions gladly give up an electron to the neighbouring nickel ions, while they themselves gladly receive an extra electron. Superexchange acts over larger distances than the direct exchange interaction, which makes this exchange so "super".

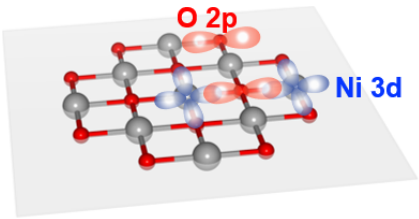

Figure 3: Visualization of the hybridization of oxygen 2p- and nickel 3d-orbitals. Nickel ions are gray, while oxygen ions are red.

2.1.2 Extensions to the Heisenberg model

While the Heisenberg Hamiltonian does an excellent job at describing magnetism through the exchange interaction, other magnetic interactions exist, which, depending on their magnitude, have to be taken into consideration. One of the more straightforward of such interactions occurs when a homogeneous magnetic field is applied in the vicinity of a system that is being studied. This magnetic field then breaks the rotational symmetry that is often present. The interaction between magnetic moments and this applied magnetic field is given through the Zeeman Hamiltonian

$$\mathcal{H}_Z = -\sum_i \mathbf{m}_i \cdot \mathbf{B}_{\text{ext}}, \tag{7}$$

where the sum runs over all sites in the lattice.

Other magnetic interactions take the form of anisotropic effects, whose sources can vary depending on their kind. Among these are the MCA, as well as the magnetic anisotropy due to dipole interactions. Physical properties in crystals are in general anisotropic, meaning that they depend on the crystallographic directions, as is the case for some magnetic effects, although there also exist important isotropic quantities, such as the Curie temperature. As a result of this magnetic anisotropy, the quantization axis takes on a preferred direction. There are various kinds of magnetic anisotropy, but the discussion here will be limited to MCA and shape anisotropy.

Whereas the origin of the exchange interaction is quantum mechanics, MCA is really a consequence of relativity. Its effects were first experimentally determined and described phenomenologically, and only later on the origin of this anisotropy was linked to the SOC, where it acts as a link between crystal symmetries and the orbital angular momentum [16]. Due to MCA, the magnetic moments in a lattice have a preferred crystallographic direction they want to lie in so that the total energy is minimized. In the presence of an external magnetic field, the spin of the electron realigns so that it minimizes the Zeeman energy, as given in equation (7). As a consequence of SOC, also the orbital angular momentum of the electron will want to start to realign, but since this is strongly coupled to the lattice, it is a bit more rigid and experiences some resistance. Most materials have a weak SOC, and hence MCA is significantly weaker than the exchange interaction, as is the case for NiO [17].

Anisotropy is typically accounted for through anisotropy constants and phenomenological models. The easiest way to do this is through uniaxial anisotropy, in which a crystal possesses a single preferred magnetization direction. In this case, the contribution to the total energy by the anisotropy is given by

$$E_{\text{uni}} = K \sin^2 \theta, \tag{8}$$

for some magnetization angle θ and the anisotropy constant K. The sign of K is important when translating this contribution into something physical. For $K > 0$, E_{Uni} has minima at $\theta = 0$ and $\theta = \pi$, indicating that the crystal is easiest to magnetize parallel to this magnetization direction. This direction is often referred to as the "easy axis", in the case that this axis coincides with the quantization axis. For the case that $K < 0$, the energy takes a minimum value in the plane of $\theta = \frac{\pi}{2}$. Physically, this means that the magnetization is free to rotate without any additional energy costs in this plane, which gives rise to "easy plane"/"hard axis" anisotropy so that the preferred magnetization direction can be anywhere within this plane.

Depending on the symmetries of the crystal, most of them possess more, and often, non-uniaxial anisotropies. For crystals with low symmetry, a second-order anisotropy contribution to the energy takes the form of

$$E = K_1 \sin^2 \theta + K_2 \sin^2 \theta \cos 2\phi, \tag{9}$$

in which K_1 and K_2 are the anisotropy constants, and θ and ϕ are the magnetization angles, which again need not necessarily be aligned with the crystallographic a, b, and c axes [18]. This description of anisotropy works well for rhombohedral and monoclinic crystals. Due to crystallographic distortions, for NiO in particular, it becomes rhombohedral [19] so equation (9) is suitable. However, these distortions are so small that they are hard to observe experimentally. Anisotropy constants can also possess some kind of dependence on internal/external stresses and strains, meaning that further deformations can occur when crystals are externally magnetized, which again is negligible for NiO.
In order to use equation (9) in the magnetic Hamiltonian, it is key to write it in a coordinate-free way, so that effectively the energy due to MCA takes the form of

$$\mathcal{H}_{MAE} = K_1 \sum_i (\mathbf{m}_i \cdot \hat{\mathbf{x}})^2 + K_2 \sum_i (\mathbf{m}_i \cdot \hat{\mathbf{y}})^2, \tag{10}$$

where $\hat{\mathbf{x}}$ and $\hat{\mathbf{y}}$ are the unit vector along the easy- and hard anisotropy axes, respectively. These unit vectors need not necessarily be the Cartesian x and y directions.

A different source for magnetic anisotropies are magnetic interactions. Magnetized crystals generate a demagnetization field which further tries to minimize the total energy [20]. Like the Coulomb interaction, magnetostatic interactions are long-ranged, meaning that this demagnetization process heavily depends on the shape and orientation of the crystals, which naturally creates easy axes within the crystal. However, these shape anisotropic effects only become relevant for systems small enough to not break up into smaller magnetic domains, where magnetization inhomogeneities play an important role, which makes this anisotropy not relevant for

NiO [21].

The interactions between electrons can to good precision be described by a magnetic dipole interaction, and also contribute to the magnetic anisotropy. From the multipole expansion in basic magnetostatics, one can compute the energy from this dipole to be [22]

$$\mathcal{H}_d = \frac{-\mu_0}{8\pi} \iint \frac{3(\mathbf{m}(\mathbf{r}_1)\cdot\mathbf{r}_{12})(\mathbf{m}(\mathbf{r}_2)\cdot\mathbf{r}_{12}) - \mathbf{m}(\mathbf{r}_1)\cdot\mathbf{m}(\mathbf{r}_2)r_{12}^2}{r_{12}^5} d^3\mathbf{r}_1 d^3\mathbf{r}_2. \tag{11}$$

Here $\mathbf{r}_{12} = \mathbf{r}_1 - \mathbf{r}_2$, $r_{12} = |\mathbf{r}_{12}|$ and $\mathbf{m}(\mathbf{r}_1)$ and $\mathbf{m}(\mathbf{r}_2)$ are the magnetic moments of each of the dipole contributions. The dipole correction generally only yields a small contribution to the total energy, allowing us to approximate its contribution, analogous to Schrön et al [23]. For transition metal oxides such as NiO this integral expression can be rewritten to a sum over the nickel sites in the crystal. Oxygen sites do not contribute to the dipole energy as their dipole moment vanishes. In this case, the dipole contribution can effectively be modeled as a uniaxial anisotropy

$$\mathcal{H}_d = K_d \sum_i (\mathbf{m}_i \cdot \hat{\mathbf{z}}_i)^2, \tag{12}$$

in which K_d is the dipole anisotropy constant, which by definition is always negative, thus leading to a hard axis anisotropy, with $\hat{\mathbf{z}}_i$ being the anisotropy axis.

Collecting all relevant magnetic interactions, the magnetic Hamiltonian in its most general form becomes

$$\begin{aligned}\mathcal{H} = -\sum_{\substack{i,j \\ i\neq j}} J_{ij}\mathbf{m}_i \cdot \mathbf{m}_j + K_1 \sum_i (\mathbf{m_i}\cdot\hat{\mathbf{x}})^2 + K_2 \sum_i (\mathbf{m_i}\cdot\hat{\mathbf{y}})^2 + \\ K_d \sum_i (\mathbf{m}_i\cdot\hat{\mathbf{z}}_i)^2 - \sum_i \mathbf{m}_i \cdot \mathbf{B}_{\text{ext}}.\end{aligned} \tag{13}$$

Simplifications can still be made when the anisotropy axes in NiO are identified, as well as determining the number of relevant exchange parameters.

2.2 Nickel oxide

NiO crystallizes in the rocksalt structure in its paramagnetic phase. For temperatures lower than its Néel temperature, NiO is AFM ordered due to the aforementioned dominant superexchange interaction [24]. Since the exchange interaction is short-ranged for insulators, like NiO, the exchange interaction can be limited to only NN and NNN exchange couplings between nickel atoms. While oxygen atoms also carry nonzero magnetic moment, they do not contribute to the total spin dynamics, due to the vanishing time-averaged magnetic moment of the oxygen atoms. The NN coupling is several orders of magnitude smaller than NNN [25], but even though they can be neglected, they are still taken into account.

NiO has different three contributions to its magnetic anisotropies, two of which are MCAs, while the other one is due to dipole interactions [23]. Calculations

have found $\langle -110 \rangle$ to be the easy anisotropy axis, which has been experimentally verified [26], however, other experiments have also found $\langle -1 - 12 \rangle$ as the easy axis [27]. Both directions are coplanar, with a negligible energy cost of rotating in this plane, so either of them can be used effectively. However, the former will be considered here since it is easiest to work with. The other two anisotropies are both hard axes, and while different in origin, they are both along the same $\langle 111 \rangle$ axes. This hard axis anisotropy forces the magnetic moments in the $\{111\}$ planes [28], which are then stacked antiferromagnetically throughout the lattice, as can be seen in figure 4 below.

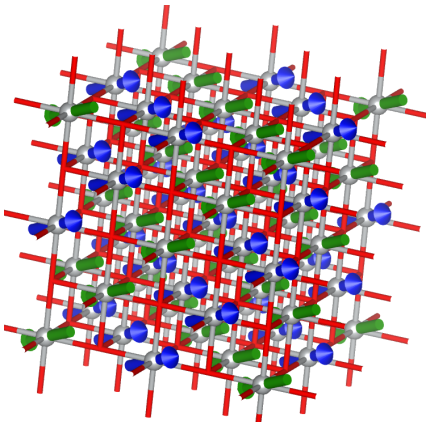

Figure 4: Crystal lattice of AFM NiO. Nickel atoms are drawn in grey, whereas oxygen atoms are drawn in red. The direction of the magnetic moments is indicated with the blue and green arrows.

2.3 Atomistic spin dynamics

Classical mechanics teaches us that a torque on a system induces a change in orbital angular momentum. Likewise, a magnetic moment in a magnetic field experiences a torque, which makes the magnetic moment precess, according to

$$\frac{d\mathbf{m}_i}{dt} = -\gamma \mathbf{m}_i \times \mathbf{B}_{\text{eff},i}, \tag{14}$$

where $\mathbf{B}_{\text{eff},i}$ is the ambient effective induced magnetic field that the magnetic moment at site i in the lattice experiences. When an external magnetic field is absent, a magnetic field is induced through the various magnetic interactions as present in the magnetic Hamiltonian, given by

$$\mathbf{B}_{\text{eff},i} = -\frac{\partial \mathcal{H}}{\partial \mathbf{m}_i}, \tag{15}$$

which generalizes the case of an externally applied magnetic field, so that equation (14) is still valid. In the absence of a damping term, this would mean that the magnetic moment would precess indefinitely, and one would not observe saturation, a reaching of thermal equilibrium, of the magnetic moment, as is experimentally observed [29]. In order to account for this, equation (14) needs to include a phenomenological dissipation term, as proposed by Gilbert in 1955, so that after some

finite time the magnetic moment would align with the effective magnetic field. The easiest way to impose this would be to slightly alter the external field to include a dissipation along the lines of

$$\mathbf{B}_{\text{eff},i} \rightarrow \mathbf{B}_{\text{eff},i} - \frac{\alpha}{\gamma m_i}\frac{\partial \mathbf{m}_i}{\partial t}, \tag{16}$$

where α is the phenomenological damping term. Inserting equation (16) into equation (14) yields

$$\frac{\mathrm{d}\mathbf{m}_i}{\mathrm{d}t} = -\gamma \mathbf{m}_i \times \mathbf{B}_{\text{eff},i} + \frac{\alpha}{m_i}\mathbf{m}_i \times \frac{\partial \mathbf{m}_i}{\partial t} \tag{17}$$

which is known as the Landau-Lifshitz-Gilbert (LLG) equation [30]. In the regime of low damping, this equation accurately describes the dynamics of magnetic moments and collective local excitations thereof, more commonly known as magnons.

2.4 Magnons in NiO

In order to arrive at an expression for the group velocity of magnons in NiO, one must solve the LLG equation for the Hamiltonian of equation (13). Under the assumptions made regarding the anisotropy and exchange interaction, the Hamiltonian becomes

$$\begin{aligned}\mathcal{H} = -J_1 \sum_{\substack{i,j\in NN \\ i\neq j}} \mathbf{m}_i \cdot \mathbf{m}_j - J_2 \sum_{\substack{i,j\in NNN \\ i\neq j}} \mathbf{m}_i \cdot \mathbf{m}_j + K_1 \sum_i (\mathbf{m_i} \cdot \hat{\mathbf{x}})^2 + \\ \tilde{K} \sum_i (\mathbf{m}_i \cdot \hat{\mathbf{y}})^2 - \sum_i \mathbf{m}_i \cdot \mathbf{B}_{\text{ext}}.\end{aligned} \tag{18}$$

Here J_1 and J_2 are the NN and NNN exchange parameters, respectively, and $\tilde{K} = K_2 + K_d$ is the hard axis anisotropy constant, which now accounts for both MCA as well as anisotropy due to dipole interactions. Ideally, one would like to include both NN and NNN exchange interactions, however in light of the complexity of the obtained magnon dispersion relation, and since $|J_2| \gg |J_1|$ because of superexchange, NN coupling will be neglected. The effective induced magnetic field, computed through equation (15), is given by

$$\mathbf{B}_{\text{eff},i} = 2J_2 \sum_{i\in NNN} \mathbf{m}_i - 2K_1(\mathbf{m}_i \cdot \hat{\mathbf{x}})\hat{\mathbf{x}} - 2\tilde{K}(\mathbf{m}_i \cdot \hat{\mathbf{y}})\hat{\mathbf{y}} + \mathbf{B}_{\text{ext}}, \tag{19}$$

which together with the LLG equation fully describes the spin dynamics within NiO. In order to obtain an expression for the magnon velocity, first, an expression for their energy needs to be derived. To achieve this, a spin-wave ansatz for the magnetic moments is made through which the corresponding dispersion relation is derived [31]. For either of the sublattices A and B, the magnetic moments take the form of

$$\begin{aligned}\mathbf{m}_i^A &= (m_{i,x}^A e^{i(qx-\omega t)}, m, m_{i,z}^A e^{i(qx-\omega t)}) \\ \mathbf{m}_i^B &= -(m_{i,x}^B e^{i(qx-\omega t)}, m, m_{i,z}^B e^{i(qx-\omega t)}),\end{aligned} \tag{20}$$

with m the magnetic moment for the nickel atom at the i-th site, ω the magnon frequency, k the wave number and x the distance of the site coupled to the i-th site.

The ansatz describes magnons traveling in the positive x direction, but for it to be valid, the amplitudes of the spin waves need to be small, i.e.

$$|m_{i,x}^{A/B}|, |m_{i,z}^{A/B}| \ll 1. \tag{21}$$

This linearizes equation (17), as this allows for products between amplitudes to be neglected, but note, however, that the solution that is obtained is an approximate one. Only couplings between lattice sites need to be considered that have a contribution parallel to the propagation direction of the excited magnon. Next, this ansatz is plugged into equation (17) and the amplitudes are collected. This linearized system of equations, in the absence of an external magnetic field, takes the form of

$$\begin{pmatrix} -\mathrm{i}\omega & X_1 & 0 & -4J_2 m\gamma \cos qa_0 \\ X_2 & -\mathrm{i}\omega & 4J_2 m\gamma \cos qa_0 & 0 \\ 0 & -4J_2 m\gamma \cos qa_0 & \mathrm{i}\omega & X_1 \\ 4J_2 m\gamma \cos qa_0 & 0 & X_2 & \mathrm{i}\omega \end{pmatrix} \begin{pmatrix} m_{i,x}^{\mathrm{A}} \\ m_{i,z}^{\mathrm{A}} \\ m_{i,x}^{\mathrm{B}} \\ m_{i,z}^{\mathrm{B}} \end{pmatrix} = 0, \tag{22}$$

where for brevity

$$\begin{aligned} X_1 &= \mathrm{i}\omega\alpha + 2(J_2 + \tilde{K})m\gamma, \\ X_2 &= -i\omega\alpha - 2(2J_2 - K_1 + \tilde{K})m\gamma \end{aligned} \tag{23}$$

have been defined. Non-trivial solutions for the magnon frequency, and hence also energy, arise when the determinant of the above matrix vanishes. Since this characteristic equation is quartic in ω, four complex solutions exist. However, two of these solutions have a negative real part and are hence non-physical solutions. The other two solutions represent the optical and acoustical magnon modes. The

$$\begin{aligned} \omega_{\pm} = \frac{1}{1+\alpha^2}(-m^2\gamma^2(8J_2(K_1 - 2\tilde{K}) + 4(K_1 - \tilde{K})\tilde{K} + K_1^2\alpha^2 + \\ 8J_2(-1+\alpha^2)(\mp K1 \cos qa_0 + J_2 \cos 2qa_0)^{1/2} \end{aligned} \tag{24}$$

2.5 Spin-spin correlation functions

Magnon spectra will play a pivotal role in the determination of the magnon velocities. In order to get a better grasp of what these spectra entail and how they are constructed, it is important to discuss some more about spin-spin correlation functions. Statistically, correlation functions merely measure how similar two quantities in a system behave. Physically, correlation functions are much more intricate, having a more widespread range of applications, varying from describing high-energy scattering processes, all the way up to the study of phase transitions [32, 33]. The field of magnetism also holds a few useful pair correlation functions. For systems in thermal equilibrium, one can measure the so-called spatial pair correlation function, which is used as a measure for the range of the magnetic order within the system. In the study of the dynamics of magnetic systems, typically thermal equilibrium is not reached and one needs to also take into account temporal fluctuations. The

pair correlation function then takes on a time dependence and is given by

$$\mathrm{C}^{\alpha\beta}(\mathbf{r},\tau) = \left\langle m^{\alpha}(\mathbf{R},t)m^{\beta}(\mathbf{R}+\mathbf{r},t+\tau)\right\rangle_{\mathbf{R},t} - \langle m^{\alpha}(\mathbf{R},t)\rangle \left\langle m^{\beta}(\mathbf{R}+\mathbf{r},t+\tau)\right\rangle_{\mathbf{R},t}, \tag{25}$$

in which the subscripts $\mathbf{R}$ and t denote averaging over all sites and observation times in the system, while superscripts α and β denote the Cartesian components of the magnetic moments. The pair correlation function hence allows for a description of how the magnetic order evolves in systems over space and time. The most prominent application of the pair correlation function comes from its ties to experiments where neutrons or electrons are inelastically scattered on magnetic systems [34]. The pair correlation function can be Fourier transformed in its spatial and temporal coordinates in order to arrive at the dynamical structure factor (DSF). The DSF is given by

$$\mathrm{S}^{\alpha\beta}(\mathbf{q},\omega) = \frac{1}{2\pi}\sum_{\mathbf{r}} e^{i\mathbf{q}\cdot\mathbf{r}} \int_{\mathbb{R}} C^{\alpha\beta}(\mathbf{r},t)e^{-i\omega t}\mathrm{d}t, \tag{26}$$

which relates the wave vectors $\mathbf{q}$ and the frequencies ω of magnons. For non-collinear systems, the DSF is a 3 by 3 matrix, however, in the case of collinear case, only the diagonal entries remain of interest. The aforementioned inelastic neutron scattering experiments only measure fluctuations perpendicular to the quantization axis of the system. Thus, when relating the DSF to experiments, one merely has to consider the orthogonal projections of the DSF to the quantization axis and relate those to the magnon excitations.

3 Spin dynamics simulations & implementation

By studying magnetism and its effects at an atomic level, one quickly enters the field of spin dynamics. Spin dynamics simulations are essential to computing magnon velocities, and as such, the Uppsala atomistic spin dynamics (UppASD) software package has been used throughout this thesis [35]. UppASD evolves the atomic magnetic moments in solids according to the previously mentioned LLG equation. Due to the small timestep used to numerically solve these equations, UppASD is ideal for the study of ultrafast magnon dynamics of AFMs, which typically have their resonance frequencies in the THz range [36]. Using various features included in UppASD, a trio of methods has been devised that allows for a good estimation of the magnon velocity.
The implementation and correct setup of NiO within UppASD is quite straightforward. NiO crystallizes in the rock salt structure, in which the nickel atoms form a face-centered cubic (fcc) lattice, which makes a primitive fcc unit cell sounds like an ideal choice to set up the simulations with. However, the presence of the oppositely directed {111} planes of atomic magnetic moments breaks the threefold rotational symmetry and could yield a more tedious working experience within UppASD. Instead, a more conventional unit cubic unit cell has been chosen, which completely nulls any potential issues in correctly setting up the MCAs and the rest of the system.

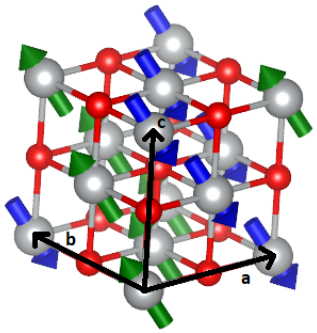

Figure 5: Implemented unit cell of NiO within UppASD. Indicated are the crystallographic a, b and c axes. Nickel- and oxygen atoms are again drawn in grey and red, respectively. The direction of the magnetic moments is indicated by the arrows.

The first of three ways to obtain the magnon velocity is by studying simulated magnon spectra, as was hinted at near the end of the previous section. UppASD contains a feature to calculate the DSF at all points for any given path through the Brillouin Zone (BZ). For this method, some small tweaks had to be done to the setup in order for UppASD to produce a correct linear spin wave spectrum, due to AFM systems initially being incompatible with the way the simulated magnon spectra were obtained [37]. Typically, a path is chosen through the BZ which passes through a lot of its high symmetry points, which are the most interesting. Since the DSF relates the magnon frequencies and wave vectors, it allows for the magnon

dispersion to be extracted from it. For each fixed wave vector $\mathbf{q}*$, the DSF $S(\mathbf{q}*, \omega)$, then, merely depending on the magnon frequency, takes the shape of a Lorentzian (or double Lorentzian in some cases), peaking at the resonance frequency of the magnons, which are to be extracted, as seen below. Additionally, the FWHM of this Lorentzian is related to the lifetime of the magnon.

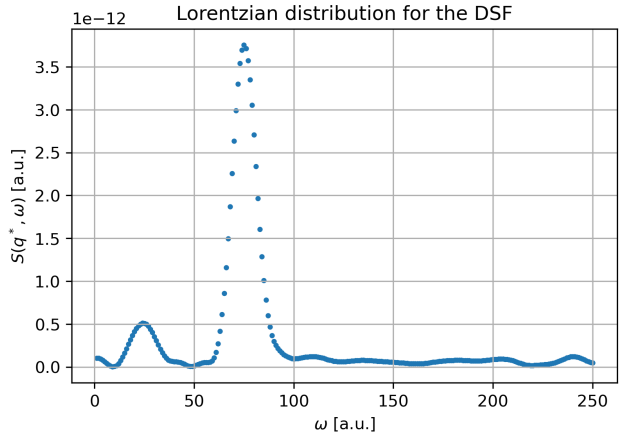

Figure 6: Lorentzian distribution of $S(\mathbf{q}*, \omega)$ as a function of ω, for a fixed wave vector $\mathbf{q}*$.

Doing this for all wave vectors included in the selected path through the BZ and collecting all the resonance frequencies, one is able to arrive at a relation between the magnon energies, up to a factor of $\hbar$, and the wave vectors.

Now that the numerical magnon dispersion is obtained, the next step is to use it to be able to compute the magnon velocity. Similar to how the wave group velocity is defined in optics, the magnon velocity is defined to be

$$\mathbf{v}_m = \frac{\partial \omega(\mathbf{q})}{\partial \mathbf{q}}, \tag{27}$$

since after all, it is a collective wavelike excitation. Note that the magnon dispersion for AFM systems needs to scale linearly with $\mathbf{q}$ for small $\mathbf{q}$ in order to get a non-vanishing group velocity in this regime [38]. This is fundamentally different than the magnon dispersion for FM systems, such as for bcc Fe, as the magnon dispersion scales quadratically with the wave vector near the center of the BZ, Γ, so that the magnon velocity vanishes. The group velocity near Γ is of particular interest, as it attains its maximum value here since dissipation plays no role due to the vanishing wave vector.
Even though the magnon velocity can be computed analytically, it translates a bit differently when computing it from the numerical data obtained through UppASD. Numerically, derivatives become slopes, so that near Γ it suffices to just compute the slope of the dispersion. Due to some troubles regarding the implementation of dissipation through complex frequencies and wave vectors, the group velocity has not been computed analytically, and instead, we resort to numerical computations. This issue will get some more elucidation in the discussion at the end.

The original paper on superluminous magnons [4] includes the magnon velocities for a small number of damping coefficients. In trying to most accurately replicate these computed superluminous magnon velocities, a wider range of damping coefficients has been used in order to extend the analysis.

The two other ways to numerically compute the magnon velocity both rely on analyzing local excitations to the magnetic structure of NiO. There exist several different ways to apply local excitations, but within the possibilities in UppASD, only two such methods have been considered. In order to mimic the setup [4] as closely as possible, the other two sets of simulations are done within a system of about 40 nm long, 4 nm wide, and 4 nm tall, which is the supposed range in which these superluminous magnon velocities can be measured.

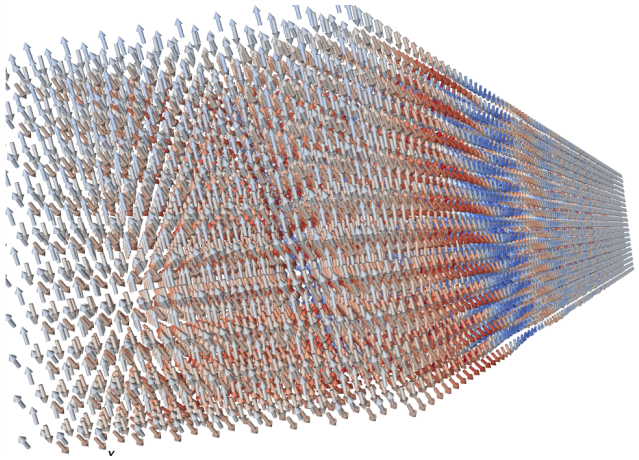

Figure 7: Snapshot of the setup used for the simulations, which consists of 100 by 10 by 10 unit cells. Different colours indicated differently directed magnetic moments, with the red and blue colours being the two extrema. A spin wave can be seen propagating through the system.

By manually flipping the direction on one, or more, magnetic moments on one end of the system, the neighbouring spins will, in turn, react to this sudden change, as they are coupled through the exchange interaction, and they themselves will start to flip. This "spin-flip" indeed excites magnons within the system, as on a bigger scale this front-end excitation starts to propagate through the system. The greater the number of magnetic moments flipped on the excited end of the system, the stronger the cascading effect will be throughout the rest of the system, and the more magnons get excited.

UppASD has the ability to track the magnetic moments of individual lattice sites over time. By selecting a specific trajectory of lattice sites in the system and tracking their magnetizations over time, a rough estimate of the time when the excitation is reached at each site can be made. Since the goal is to study magnon propagation over nanoscale distances, the relevant path is chosen to be in the center of the front end, along the length of the system. For one such sites, the magnetization evolves

like figure 8a below.
The "excitation time", as indicated by the red cross in both plots in figure 8, is determined at which point in time the magnetization deviates more than a set relative amount from the initial value at the start of the simulation. As a nice cross-check, one can see that the magnetization over time slowly starts restabilizing around its ground state value, as is physically expected. The magnon velocity at the j-th site away from the excitation can simply be computed as

$$v_{m,j} = \frac{ja_0}{\tau_j}, \tag{28}$$

where a_0 is the lattice parameter of NiO and τ_j is the excitation time at the j-th site.

Aside from spin-flips, magnons can also be excited thermally, or due to externally applied magnetic fields. The second way magnons are excited in this thesis is through externally pulsing a magnetic field on one end of the system. In order to stay as close to the pulsing in [4] as possible, the pulsing in UppASD is done with an externally applied harmonic magnetic field with an angular frequency in the THz range. Moreover, the pulsing time is 120 fs, and a large magnitude has been applied in order to fully saturate the excited end. Similar to the spin-flip, the magnetization of specific sites can be tracked in order to estimate the excitation time, after which again the magnon velocity at specific sites can be computed through equation (28). While pulses are repeated at a certain frequency in [4], the decision has been made to limit the number of pulses to one, as to guarantee only individual excited magnons are observed.

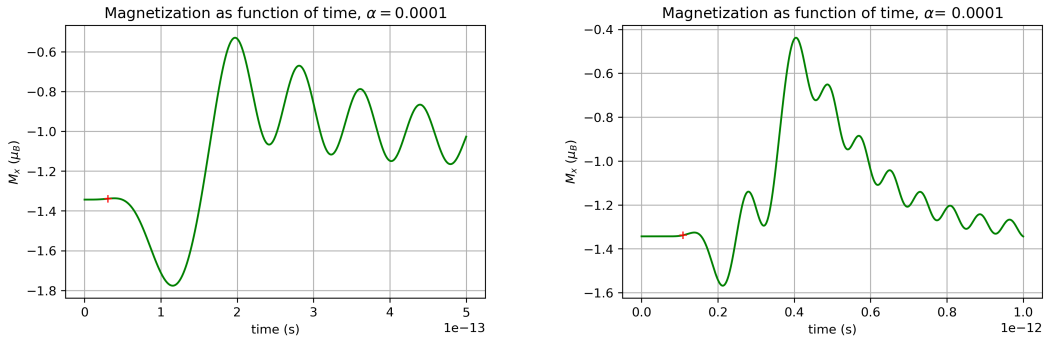

(a) (b)

Figure 8: (a), Magnetization as a function of time for a specific lattice site in the system. Indicated with the red cross is the time at which the spin-flip excitation has reached this site. (b), Magnetization as a function of time for a specific lattice site in the system. Indicated with the red cross is the time at which the pulsed magnetic excitation has reached this site. Note that this lattice site need not necessarily be the same one.

4 Results

Ideally, one would like to exhaust all possible ways to determine the magnon velocity in order to maximize the reliability of the simulations. More methods for exciting magnons exist, such as introducing impurities in the magnetic lattice as it would destabilize the magnetic order. This would excite singular magnons, which quickly dissipate over time as the magnetic order is re-established. However, considering the number of methods that are used, the three methods should deem adequate in order to give a sufficiently accurate judgement on the behaviour of magnon velocities at nanoscale length scales. This section will present and analyse the simulation results of each of the three methods.

4.1 Magnon spectra

Naturally, one starts by looking for abnormal magnon behaviour on the biggest scale and slowly tries to narrow it down. For a start, the spectrum of bulk NiO is simulated and investigated. Its theoretical magnon spectrum is readily available [39], allowing for easy comparisons between the two of them. One should note that the theoretical spectrum uses slightly higher values for the exchange parameters, as a slightly different system is studied there, which accounts for the slightly smaller simulated magnon spectra. This would in turn also result in slightly smaller magnon velocities. The path traversed through the truncated octahedral BZ of the fcc unit cell passes several high symmetry points as indicated by the labels along the x-axis.

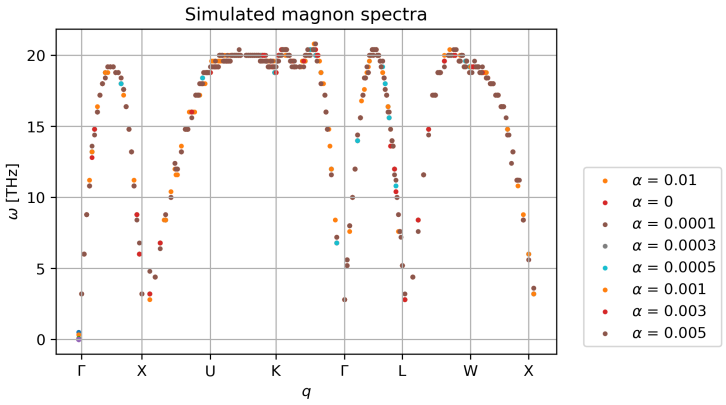

Figure 9: Simulated magnon spectrum for bulk NiO for various damping coefficients.

At first glance, these spectra do not look out of the ordinary, and though a different path through the BZ is taken as compared with the theoretical spectrum, the general shape agrees rather well. Even more so, the spectra overlap for the various damping coefficients, indicating that the magnon dispersion seems to have a relatively weak dependence, if any at all, on the damping coefficients. Computing the magnon velocity through the slope of the spectra close to Γ for these bulk spectra hence gives again a not-so-surprising result.

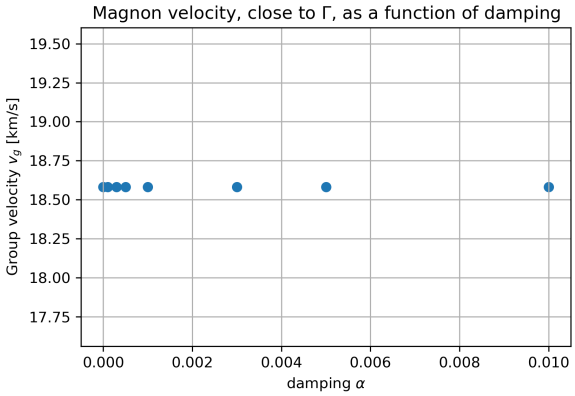

Figure 10: Magnon velocity as a function of damping for the bulk spectra.

The magnon velocities appear independent of the damping coefficient, but this might be due to a lower sampling frequency, as is elaborated on in the discussion. Moreover, their magnitudes are a bit lower than previous determinations of magnon velocities in NiO [34, 40], but when taking into account the extra factor that deviates the simulated spectra from the experimental ones, they are in good agreement.

Suggested in [4] is that these superluminous magnon velocities occur only for magnons with rather small wave vectors, and hence large wavelengths, in the range of several 10^6 cm^{-1}. More simulations of bulk NiO are done with an increased system size which allows for these long wavelength magnons to be properly sampled.

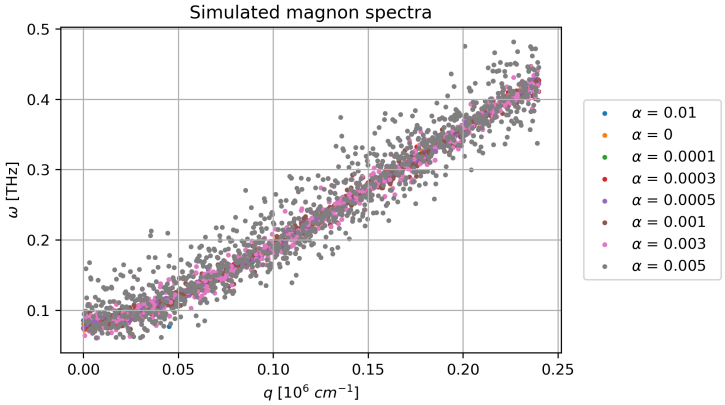

Figure 11: Simulated magnon spectra with an increased resolution for smaller wave vectors.

Once more, the simulated spectra for simulations with nonzero damping show no deviating behaviour from the undamped one, as they all still overlap. Their shapes and energy ranges are well in accordance with previous theoretical works [41]. For increasing damping, the spectra start becoming less clear and more scattered, which is to be expected, as bigger damping ensures a faster return of the system to its ground state so that it stops properly contributing to the spin-spin correlation functions. These spectra are fitted in the "tail", which is the steepest part of the

spectrum, and hence visually should yield the highest possible magnon velocity, as is done in the figure below.

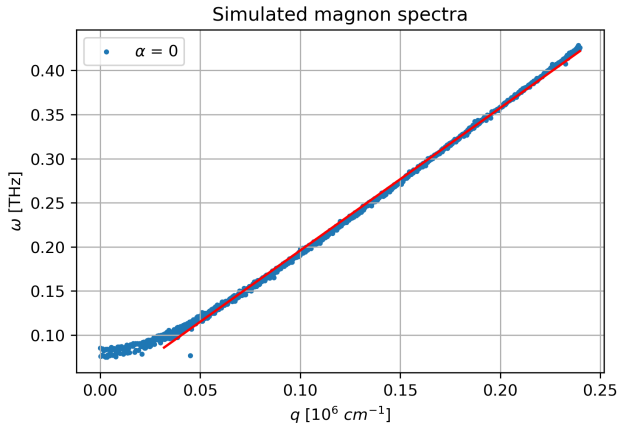

Figure 12: Linearly fitted (red) simulated magnon spectrum for small wave vectors.

Attempts to plot the acoustical magnon mode from equation (24) have been done, but these were unsuccessful and have been commented on in the discussion. Collectively, this yields the following plot for the magnon velocity for the various damping coefficients.

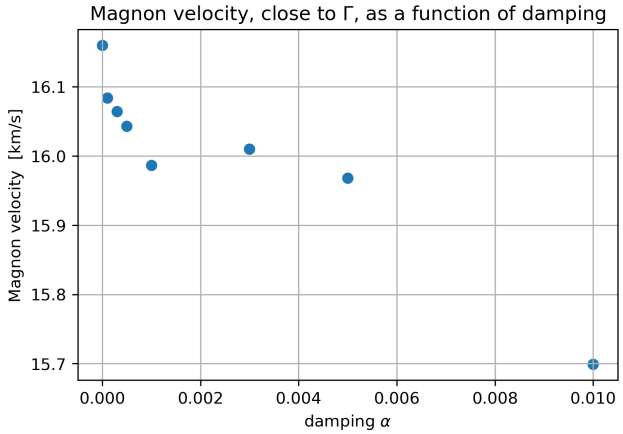

Figure 13: Magnon velocity as a function of damping for the small wave vector spectra.

Although seemingly minimal, there seems to be a downward trend of the magnon velocity for increasing damping, which is what is classically expected. The presence of damping allows for the dissipation of energy, which classically should not yield increasing magnon velocities. This is observed, as the maximum magnon velocity occurs for the undamped case. Furthermore, these computed magnon velocities come nowhere close to exceeding this "superluminous barrier" of measuring at least one order of magnitude over the current known magnon velocity in NiO. From analysing the various magnon spectra within NiO, it can, however, be established

that the magnon velocity does not depend on the damping in such a way that it allows for this superluminous behaviour to occur.

4.2 Local spin-flips

Due to its instantaneous nature, the spin-flip excitation might not be the most physically realizable one, but it will still prove to be useful to study magnon dynamics. Instead of flipping a singular magnetic moment on one end of the system, simulations are done where the entire front plane is flipped in order to strengthen the effects of the excitation. For the same set of damping coefficients, the magnon velocities at the lattice sites away from the initial excitation are computed.

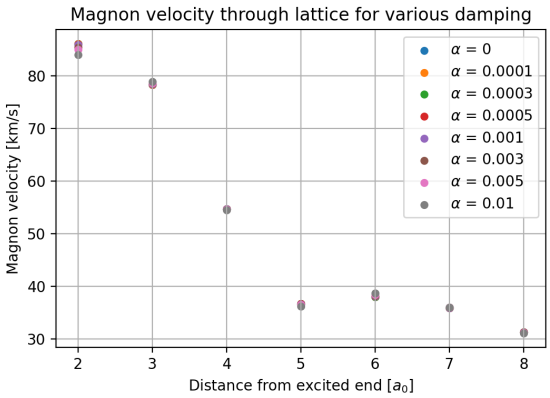

Figure 14: Magnon velocity as a function of the interatomic distance due to a spin-flip excitation, for various damping coefficients.

Note that the first site after the excitation is missing from this plot. It turns out that the spin-flip excitation transfers the excitation infinitesimally fast to its NN. Due to this non-harmonic behaviour, the excited magnon would then reach velocities that are physically not realistic, which is enough to exclude it. As such, the NNN of the excited site would then act as the site at which the maximum physical magnon velocity can be computed through the simulations, under the logical assumption that the NN will still hold the actual maximum velocity, which is then slightly higher. Moreover, the magnon velocity yet again looks like it is minimally dependent on the damping coefficient. The maximum computed magnon velocity is slightly higher than double that of the maximum magnon velocity as observed in the bulk NiO spectrum. In some way, this is strange as there do not exist different kinds of magnons, as all magnons are expected to propagate with the same maximum velocity. One can also see that the magnon velocity steadily decreases as it propagates through the system, up to the point where it starts to settle at around 30 km/s, which is nicely in accordance with the computed bulk magnon velocity. The magnon decelerates due to the energy dissipation, but its deceleration rapidly decreases after it has passed several lattice sites. Some inconsistencies in the decreasing trend seem to occur at the sixth site from the excitation where the magnon velocity increases, but this interesting result can be quickly negated by noting that the simulations also include an external stochastic field, which accounts

for randomness in the simulations. The most notable observation from studying this spin-flip excitation, however, remains the low dependence of the magnon velocity on the damping coefficient. This agrees nicely with the classical theory as well as with the conclusions from the observed magnon spectra. Simulations have also been done with large systems in order to capture the behaviour of low wavelength magnons, however, these produced no new results.

4.3 Pulsed magnetic excitations

Magnon excitations due to a pulsed externally applied magnetic field most closely resemble the experiment in [4] and therefore make for the most promising attempt to try to reproduce its results. This excitation is physically more realizable than the spin-flip, and due to its harmonic time dependence, this excitation does not transfer infinitesimally fast onto its NN. As a result, the NN site will be able to measure a physical and useful magnon velocity. Interestingly, as the magnetic pulse starts, the magnetic moments on the excited end start spinning out of control up to the point where the pulse ends, after which they slowly restabilize back into the ground state.

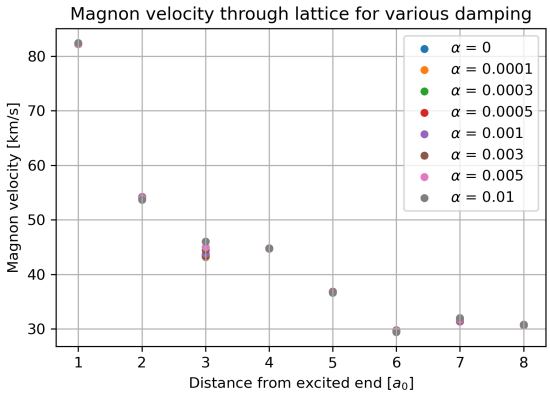

Figure 15: Magnon velocity as a function of the interatomic distance due to a pulsed magnetic excitation, for various damping coefficients.

This figure looks very similar to figure 14, which checks out nicely with the results from the spin-flip, though one should not forget that the latter excludes one lattice site. Once more, the magnon velocities seem independent on the damping coefficients, as indicated by the strong overlap of the velocities at each lattice site. The maximum computed velocity reaches about the same as for the spin-flip, coming nowhere near exceeding the bulk magnon velocity and entering the superluminous regime. As the excitation propagates through the system, the velocity saturates again at around the value it has in bulk, which is consistent with what was found before.

5 Conclusion and Outlook

In this thesis, spin dynamics simulations in NiO are done as a response to previous experimental work where magnon velocities were measured that exceeded previous theoretical maxima by significant amounts, in order to verify their existence. A classical derivation of the magnon spectrum within NiO, supported by simulations of the magnon spectra for high wavelength magnons, both show no anomalous behaviour for the magnon velocities. Magnon velocities remain in the same order of magnitude as previously experimentally determined values, coming nowhere near the value of the superluminous magnons. Moreover, the magnon dispersion is more or less independent of the damping coefficients, whence the superluminous magnons supposedly originated, only showing a small decrease in the magnon velocity for increasing damping coefficients, which agrees with the classical expectations. Magnons are excited and tracked over nm distances by locally flipping individual magnetic moments, as well as ultrafast externally pulsed magnetic fields. Maximally computed magnon velocities are slightly higher than the values they would have been in bulk, but again show no superluminous behaviour and remain relatively independent of the damping coefficients. Moreover, these magnon velocities rapidly decelerate back to their bulk values, which is consistent with previously obtained results.

While additional simulations could be done that determine the magnon velocity in alternative ways, it remains to be seen to what extent these would produce new results. Previous methods all indicate that the presence of damping in the LLG cannot be the origin of these superluminous magnons. This then raises the question of what could instead be their source, if they exist at all. It might be interesting to apply an external pulsed magnetic field in the center of the system and see the magnon dynamics that arise from that, in order to compare with the spin dynamics simulations in [4]. Obtained results agree with an alternative approach, which is fundamentally different, as it is quantum mechanical in nature, in which magnetic moments are mapped to bosonic creation and annihilation operator as per the Holstein-Primakoff transformations. Here, the magnon dispersion is computed straight from diagonalizing the magnetic Hamiltonian. This avoids the magnonic dissipation in the LLG altogether, while energy dissipation to electrons and phonons may still be included, which again produces no superluminous magnons [41].

It might be interesting to attempt to recreate the original experiment in which superluminous magnons are measured in order to rule out any experimental mistakes and inaccuracies. Any failed attempts to recreate superluminous magnon would then immediately rule out their existence. Spin dynamics simulations are also done in [4] in order to support their findings regarding superluminous magnons, however, a different code is used than UppASD. It might be worth trying to repeat the various methods to determine magnon velocity, but this time using the spin dynamics code that was used in the original paper.

6 Discussion

A thorough analysis of the magnon velocity in NiO using UppASD has shown no existence of superluminous magnons. Still, two different conclusions are drawn in two different studies, which require some discussion and clarification.

Starting off with the experimental part [4], just like any other experiment, it is prone to mistakes, inaccuracies, and uncertainties. A potential reason for measuring significantly higher magnon velocities than expected is that the skin depth of the laser is too large, which means that it penetrates the FM, as seen in figure 2. As a result, the laser, although briefly, excites spin currents prematurely. This results in a premature magnon current, which in turn also makes the NM emits a premature signal so that measured magnon velocities become slightly inaccurate. Additionally, there is a possibility for interface effects between the various elements of the trilayer, which could influence the velocities of the different kinds of currents that arise through the various layers.

Spin dynamics simulations are also done in [4]. Here, instead of exciting the one end of the setup with externally pulsed magnetic fields, the center is excited, which is odd, since mimicking their experimental setup seems well within the capabilities of their code. Due to the unknown nature of the code that has been used, no further comments can be made. Supporting their results from the simulations are the analytically derived magnon dispersion and magnon velocity. In order to take into account the dissipative nature of the magnon dynamics, one has to complexify either the magnon frequencies or magnon wave vectors, which ended up being a bit more tedious to work with than expected. While the analytical magnon dispersion can be reproduced, troubles arise when trying to obtain the magnon velocities. Interesting to note is that the derivation is done only using the NNN exchange coupling, which is justified due to the dominant superexchange. Even though this might account for some inaccuracy in the magnon spectra, it does not account for a fundamentally different magnon behaviour. If one decides to work with a complex wave vector, equation (27) can be used to derive the magnon velocity, with the subtle change that one needs to take the derivative with respect to the projection along the real part of the wave vector. Attempts to do this with the magnon dispersion in equation (24) have been done using Mathematica, however, no functional form similar to the ones in [4] have been reached. Since no additional information regarding the derivation is supplied, it makes it a bit dubious, while still, the analytical magnon velocity matches nicely with the spin dynamics simulations. Moreover, the spin dynamics simulations for various damping coefficients do not all sample the same wavelength magnons. This should be at the expense of the predictive power of the low wave vector magnon spectra, but, maybe unrightfully, conclusions are still drawn.

Small inaccuracies also occurred during the analysis using UppASD, however, none of which are able to substantially influence the general obtained results. The simulated magnon spectra contain some "dead points". For these points, $S(\mathbf{q}*, \omega)$ does not measure a proper signal, resulting in incorrectly computed resonance frequencies, which in the end need to be filtered out. This makes it seem like the magnon

spectra have a low sampling frequency in some ranges. The determination of the magnon velocity using the magnon spectra relied on fitting data points twice, once in the determination of resonance frequencies, and the other in the actual determination of the magnon velocity. For poor data, these fits often converged pretty poorly. Instead on most occasions, the maxima of the DSF were used to avoid having to fit it with a Lorentzian, which mostly improved the obtained results for the magnon velocity. The theoretically derived magnon dispersion also does not quite match the simulated results. While being in the correct order of magnitude for the magnon frequencies, the value at Γ is significantly lower for the simulated magnon spectra, which indicates that something might have gone wrong when setting up the anisotropies. Moreover, the simulated magnon spectra are much steeper than the theoretical ones, which then yields much higher magnon velocities for the former. Since the magnon velocities from the simulated magnon spectra are corresponding quite well to previous experimental work, one can conclude that something erroneous occurs in the theoretical derivation of the magnon dispersion. Furthermore, in the analysis of studying locally excited magnons, the excitation times were susceptible to the chosen absolute error. This usually resulted in a few extra/less km/s of the magnon velocity at each lattice site. The same phenomenon occurred when different projections of the magnetization at each lattice site were chosen, however, yet again this only resulted in a minor difference in the magnon velocity. Lastly, one limitation of the latter two methods is that only the magnon velocity could be computed on the individual lattice sites, which resulted in rather discrete plots for the magnon velocity. It would have made the analysis more complete if a more continuous interval could be considered.

Acknowledgements

The spin dynamics simulations were enabled by resources provided by the Swedish National Infrastructure for Computing (SNIC), partially funded by the Swedish Research Council through grant agreement no. 2018-05973.
Furthermore, I want to thank Lina for her nice doodle and wonderful Swedish translation, as well as Oscar and Anders for the fun times and their great help regarding magnetism and UppASD. I don't think there exists a better pair of supervisors:)

References

[1] S. Mørup, M. Hansen, and C. Frandsen, "1.14 - Magnetic Nanoparticles," in *Comprehensive Nanoscience and Technology*, pp. 437–491, Academic Press, 2011.

[2] M. Ziese and M. J. Thornton, "Spin electronics," 2007.

[3] H. Yan, Z. Feng, P. Qin, X. Zhou, H. Guo, *et al.*, "Electric-Field-Controlled Antiferromagnetic Spintronic Devices," *Advanced Materials*, vol. 32, no. 12, p. 1905603, 2020.

[4] K. Lee, D.-K. Lee, D. Yang, R. Mishra, D.-J. Kim, *et al.*, "Superluminal-like magnon propagation in antiferromagnetic NiO at nanoscale distances," *Nature Nanotechnology*, vol. 16, pp. 1337–1341, December 2021.

[5] X. R. Wang, "Anomalous spin Hall and inverse spin Hall effects in magnetic systems," *Communications Physics*, vol. 4, no. 1, pp. 1–6, 2021.

[6] T. Kampfrath, A. Sell, G. Klatt, A. Pashkin, *et al.*, "Coherent terahertz control of antiferromagnetic spin waves," *Nature Photonics*, vol. 5, no. 1, pp. 31–34, 2011.

[7] L. J. Wang, A. Kuzmich, and A. Dogariu, "Gain-assisted superluminal light propagation," *Nature*, vol. 406, no. 6793, pp. 277–279, 2000.

[8] I. Dzyaloshinsky, "A thermodynamic theory of "weak" ferromagnetism of antiferromagnetics," *Journal of physics and chemistry of solids*, vol. 4, no. 4, pp. 241–255, 1958.

[9] T. Moriya, "Anisotropic superexchange interaction and weak ferromagnetism," *Physical review*, vol. 120, no. 1, p. 91, 1960.

[10] A. Zee, "Group theory in a nutshell for physicists," 2016.

[11] A. I. Liechtenstein, M. Katsnelson, V. Antropov, and V. Gubanov, "Local spin density functional approach to the theory of exchange interactions in ferromagnetic metals and alloys," *Journal of Magnetism and Magnetic Materials*, vol. 67, no. 1, pp. 65–74, 1987.

[12] A. Szilva, M. Costa, A. Bergman, L. Szunyogh, L. Nordström, and O. Eriksson, "Interatomic exchange interactions for finite-temperature magnetism and nonequilibrium spin dynamics," *Physical review letters*, vol. 111, no. 12, p. 127204, 2013.

[13] M. Katsnelson and A. Lichtenstein, "First-principles calculations of magnetic interactions in correlated systems," *Physical Review B*, vol. 61, no. 13, p. 8906, 2000.

[14] W. Nolting and A. Ramakanth, "Quantum theory of magnetism," 2009.

[15] P. W. Anderson, "New approach to the theory of superexchange interactions," *Physical Review*, vol. 115, no. 1, p. 2, 1959.

[16] J. H. van Vleck, "On the anisotropy of cubic ferromagnetic crystals," *Physical Review*, vol. 52, no. 11, p. 1178, 1937.

[17] J. Zavašnik, A. Šestan, and V. Shvalya, "Microscopic techniques for the characterisation of metal-based nanoparticles," in *Comprehensive Analytical Chemistry*, vol. 93, pp. 241–284, Elsevier, 2021.

[18] R. Skomski, "Simple models of magnetism," 2008.

[19] W. Roth, "Multispin axis structures for antiferromagnets," *Physical Review*, vol. 111, no. 3, p. 772, 1958.

[20] J. M. Coey, "Magnetism and Magnetic Materials," 2010.

[21] T. Paine, L. Mendelsohn, and F. Luborsky, "Effect of shape anisotropy on the coercive force of elongated single-magnetic-domain iron particles," *Physical Review*, vol. 100, no. 4, p. 1055, 1955.

[22] J. D. Jackson, "Classical Electrodynamics," 1998.

[23] A. Schrön, C. Rödl, and F. Bechstedt, "Crystalline and magnetic anisotropy of the 3 d-transition metal monoxides MnO, FeO, CoO, and NiO," *Physical Review B*, vol. 86, no. 11, p. 115134, 2012.

[24] N. Rinaldi-Montes, P. Gorria, D. Martínez-Blanco, A. B. Fuertes, I. Puente-Orench, L. Olivi, and J. A. Blanco, "Size effects on the Néel temperature of antiferromagnetic NiO nanoparticles," *AIP advances*, vol. 6, no. 5, p. 056104, 2016.

[25] Y. O. Kvashnin, O. Grånäs, I. Di Marco, M. Katsnelson, A. Lichtenstein, and O. Eriksson, "Exchange parameters of strongly correlated materials: Extraction from spin-polarized density functional theory plus dynamical mean-field theory," *Physical Review B*, vol. 91, no. 12, p. 125133, 2015.

[26] W. L. Roth and G. A. Slack, "Antiferromagnetic Structure and Domains in Single Crystal NiO," *Journal of Applied Physics*, vol. 31, no. 5, pp. S352–S353, 1960.

[27] J. Baruchel, M. Schlenker, K. Kurosawa, and S. Saito, "Antiferromagnetic S-domains in NiO," *Philosophical Magazine B*, vol. 43, no. 5, pp. 853–860, 1981.

[28] S. M. Rezende, A. Azevedo, and R. L. Rodríguez-Suárez, "Introduction to antiferromagnetic magnons," *Journal of Applied Physics*, vol. 126, no. 15, p. 151101, 2019.

[29] P. Monod, J. Prejean, and B. Tissier, "Magnetic hysteresis of CuMn in the spin glass state," *Journal of Applied Physics*, vol. 50, no. B11, pp. 7324–7329, 1979.

[30] O. Eriksson, A. Bergman, L. Bergqvist, and J. Hellsvik, "Atomistic Spin Dynamics: Foundations and Applications," 2017.

[31] C. Kittel and P. McEuen, "Introduction to solid state physics," 1996.

[32] E. V. Shuryak, "Correlation functions in the QCD vacuum," *Reviews of Modern Physics*, vol. 65, no. 1, p. 1, 1993.

[33] N. Hasselmann, A. Sinner, and P. Kopietz, "Two-parameter scaling of correlation functions near continuous phase transitions," *Physical Review E*, vol. 76, no. 4, p. 040101, 2007.

[34] M. T. Hutchings and E. Samuelsen, "Measurement of spin-wave dispersion in NiO by inelastic neutron scattering and its relation to magnetic properties," *Physical Review B*, vol. 6, no. 9, p. 3447, 1972.

[35] J. Hellsvik, L. Bergqvist, A. Bergman, and J. Chico et al, *UppASD*. Uppsala, Sweden.

[36] J. Li, C. B. Wilson, R. Cheng, M. Lohmann, M. Kavand, W. Yuan, *et al.*, "Spin current from sub-terahertz-generated antiferromagnetic magnons," *Nature*, vol. 578, no. 7793, pp. 70–74, 2020.

[37] S. Toth and B. Lake, "Linear spin wave theory for single-Q incommensurate magnetic structures," *Journal of Physics: Condensed Matter*, vol. 27, no. 16, p. 166002, 2015.

[38] S. Mu, R. P. Hermann, S. Gorsse, H. Zhao, M. E. Manley, R. S. Fishman, and L. Lindsay, "Phonons, magnons, and lattice thermal transport in antiferromagnetic semiconductor MnTe," *Physical Review Materials*, vol. 3, no. 2, p. 025403, 2019.

[39] P. Maldonado and Y. O. Kvashnin, "Microscopic theory of ultrafast out-of-equilibrium magnon-phonon dynamics in insulators," *Physical Review B*, vol. 100, no. 1, p. 014430, 2019.

[40] O. Gomonay, T. Jungwirth, and J. Sinova, "High antiferromagnetic domain wall velocity induced by Néel spin-orbit torques," *Physical review letters*, vol. 117, no. 1, p. 017202, 2016.

[41] S. Rezende, R. Rodríguez-Suárez, and A. Azevedo, "Diffusive magnonic spin transport in antiferromagnetic insulators," *Physical Review B*, vol. 93, no. 5, p. 054412, 2016.